ADVANCED FUNCTIONAL MATERIALS
www.afm-journal.de

Molecular Storage of Mg Ions with Vanadium Oxide Nanoclusters

Yingwen Cheng, Yuyan Shao, Vadivukarasi Raju, Xiulei Ji, B. Layla Mehdi, Kee Sung Han, Mark H. Engelhard, Guosheng Li, Nigel D. Browning, Karl T. Mueller, and Jun Liu**

Mg batteries have potential advantages in terms of safety, cost, and reliability over existing battery technologies, but their practical implementations are hindered by the lack of amenable high-voltage cathode materials. The development of cathode materials is complicated by limited understandings of the unique divalent Mg^{2+} ion electrochemistry and the interaction/transportation of Mg^{2+} ions with host materials. Here, it is shown that highly dispersed vanadium oxide (V_2O_5) nanoclusters supported on porous carbon frameworks are able to react with Mg^{2+} ions reversibly in electrolytes that are compatible with Mg metal, and exhibit high capacities and good reaction kinetics. They are able to deliver initial capacities exceeding 300 mAh g^{-1} at 40 mA g^{-1} in the voltage window of 0.5 to 2.8 V. The combined electron microscope, spectroscopy, and electrochemistry characterizations suggest a surface-controlled pseudocapacitive electrochemical reaction, and may be best described as a molecular energy storage mechanism. This work can provide a new approach of using the molecular mechanism for pseudocapacitive storage of Mg^{2+} for Mg batteries cathode materials.

Dr. Y. Cheng, Dr. Y. Shao, Dr. G. Li, Dr. J. Liu
Energy and Environment Directorate
Pacific Northwest National Laboratory
Richland, WA 99352, USA
E-mail: yuyan.shao@pnnl.gov; jun.liu@pnnl.gov
Dr. Y. Shao, Dr. B. L. Mehdi, Dr. K. S. Han, Dr. N. D. Browning, Dr. K. T. Mueller, Dr. J. Liu
Joint Center for Energy Storage Research (JCESR)
Pacific Northwest National Laboratory
Richland, WA 99352, USA
Dr. V. Raju, Prof. X. Ji
Department of Chemistry
Oregon State University
Corvallis, OR 97331, USA
Dr. B. L. Mehdi, Dr. N. D. Browning, Dr. K. T. Mueller
Physical and Computational Sciences Directorate
Pacific Northwest National Laboratory
Richland, WA 99352, USA
Dr. K. S. Han, Dr. M. H. Engelhard, Dr. K. T. Mueller
Environmental Molecular Sciences Laboratory (EMSL)
Pacific Northwest National Laboratory
Richland, WA 99352, USA
Dr. N. D. Browning
Department of Materials Science and Engineering
University of Washington
Seattle, WA 98195, USA
Dr. K. T. Mueller
Department of Chemistry
Pennsylvania State University
University Park, PA 16802, USA

DOI: 10.1002/adfm.201505501

1. Introduction

Rechargeable batteries based on magnesium (Mg) metal have been recognized as one of the most viable candidates for post Li-ion energy storage. Compared with other widely pursued metal anodes such as lithium and sodium, Mg metal has a higher volumetric capacity (3833 mAh cm^{-3}), lower cost, and much better safety characteristics.[1] In addition, the electrochemical deposition of Mg^{2+} ions does not involve formation of dendritic structures and has close to 100% coulombic efficiency when operated in the recently developed advanced electrolytes.[2] These characteristics suggest that Mg metal holds great promises for durable, safe, and high energy density energy storage devices.[3] The practical realization of Mg batteries, however, is currently limited by two major challenges and several other issues. First, the reversible deposition and stripping of Mg^{2+} ions require specially synthesized electrolytes that will not form surface passivation layers, which are believed to block Mg^{2+} ion transport.[1b] These electrolytes, such as those based on magnesium organoborate and organohaloalumiates, are usually corrosive and have much narrower stable voltage window compared with Li^+ and Na^+ battery electrolytes.[4] Recent developments, particularly on the all-phenyl-complex electrolytes,[5] the all-inorganic electrolytes,[6] and the non-halide electrolytes,[7] have established electrolytes with significantly improved voltage stability and activity. They provide viable approaches to search for high-voltage cathode materials when combined with the use of stable cathode current collectors such as Mo and W.[8]

The second major challenge is the lack of amenable high-voltage cathode materials. Conventional intercalation cathode materials developed for Li and Na batteries (such as layered and spinel oxides, and olivine phosphates) were found to have poor reactivity with Mg^{2+} ions.[1b,2,9] This is likely due to the much higher charge density associated with divalent Mg^{2+} ions that brings stronger coulombic interaction with the host materials and results in poor ionic transport and difficulties in structural stabilization.[9b] Cluster type compounds that have the mechanism of delocalizing electrons for efficient attainment of local electroneutrality, such as the Chevrel phase and fullerenes, were demonstrated to have good reactivity with Mg ions but both their voltage (<2.0 V) and capacity (<100 mAh g^{-1}) are quite

low.[10] Recently, MnO_2 was found to have decent capacities of ≈250 mAh g^{-1} at low rates and the mechanism was identified as the conversion reaction through formation of amorphous MgO and MnO_x.[11] These provide important insights on the cathode materials transformation mechanism but both the reversibility and stability need substantial improvements.[12] Another approach involves engineering the spacing of layered materials,[13] such as using polyethylene oxide for MoS_2[14] and MoO_3.[13] This approach allows control of the Mg^{2+} ions–host material interaction and improves the intercalation kinetics but the voltages are still quite limited. Overall, despite these great progresses, there are very few demonstrations of high-voltage Mg cathode materials that are compatible with Mg metal and Mg electrolytes, and further materials advancements are required.

Recent studies on the electrochemistry of novel electrode materials, such as bismuth nanotubes,[15] tin–antimony alloys,[16] and Mo_6S_8 Chevrel phase nanocubes,[10a] revealed that nanostructuring is a particularly important approach for Mg batteries. Previously, the V_2O_5 family of materials with different morphology, phase and structure has been widely studied for energy storage.[17] Several studies showed decent reactivity of Mg^{2+} ions with certain V_2O_5 materials, such as nanocrystalline V_2O_5,[18] V_2O_5 gel,[19] and V_2O_5 gel/carbon composite.[20] These studies have concluded that the shielding of Mg^{2+} divalent charge with water molecules (in the solvent and/or in V_2O_5 crystal structure) is necessary for the reactivity.[9b] Such an approach of using water to assist Mg intercalation, however, is problematic for a Mg metal anode because water can react with the Mg metal and form passivation films.[21] Recently, both crystalline and amorphous ultrathin layers of V_2O_5 were reported to have superior reactions with Li^+ and/or Na^+ ions.[22] In addition, Arthur et al. developed the use of amorphous V_2O_5–P_2O_5 powders for Mg battery cathodes with enhanced Mg^{2+} ions diffusion and high voltage reversiblity.[23] The rational combination of these previous works suggests that nanosized V_2O_5 could be a good platform to study the reaction of metal oxides with Mg^{2+} ions.

In this work we focus on studying the composite materials of highly dispersed V_2O_5 nanoclusters supported on porous carbon for hosting Mg ions. This composite material was synthesized using the ambient hydrolysis deposition (AHD) method as has been described in a previous work.[22c] The porous carbon support was synthesized using the well-established protocol with resorcinol and formaldehyde as precursors (referred as RFC).[24] The proper combination of the unique AHD method and porous carbon support affords composite materials with uniformly surface-coated V_2O_5 clusters.[22c] The weight ratio of V_2O_5 in the composite material can be readily controlled over a wide range (20–80 wt%) by the number of AHD cycles.

2. Results and Discussion

In this work, we focused on the composite with ≈45 wt% of V_2O_5 because the previous study has showed that this composition works best for reversible storage of Na^+ ions.[22c] The characterizations of the composites with thermogravimetric analysis (TGA, for V_2O_5 loading) and low magnification transmission electron microscopy (TEM)/ energy-dispersive X-ray spectroscopy (EDS) shows uniform V_2O_5 coatings within the RFC framework.[22c] The characterizations performed in this work aim at understanding the detailed structure of V_2O_5 and its interaction with the carbon support. **Figure 1**a,b compare typical high-resolution TEM images acquired from RFC and the RFC/V_2O_5 composite. These two materials show similar features and have wrinkled lattice fringes that can be attributed to poorly crystalline carbon.[25] Interestingly, the supported V_2O_5 did not show well-defined lattice fringes and therefore should be interpreted as amorphous materials. This agrees with the X-ray diffraction (XRD) results of only showing a very broad and weak peak at ≈26° as will be discussed below. Considering the fact that V_2O_5 had a high loading of ≈45 wt%, we believe that they were highly dispersed and therefore we term them as nanoclusters since the size was on the order of few nanometers. This is further supported with scanning TEM (STEM) imaging

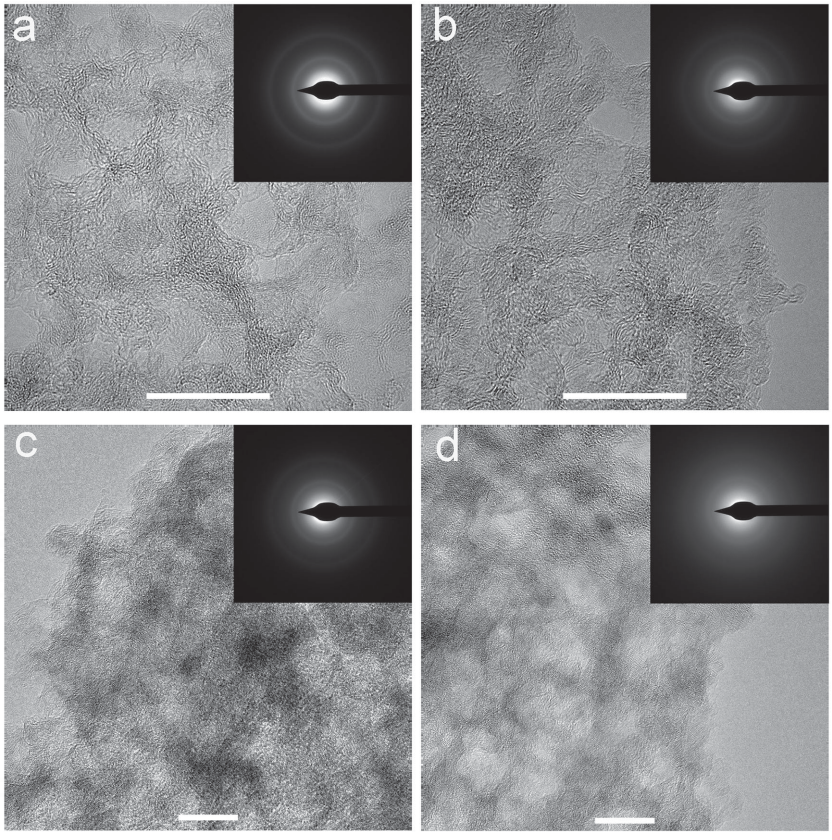

Figure 1. TEM images and selected area electron diffraction (SAED, inset) of a) RFC, b) pristine, c) magnesiated, and d) demagnesiated RFC/V_2O_5 composites. The morphology of these samples was similar, and the vanadium oxide nanoclusters were in a highly dispersed state as no clear lattice fringes other than those from poorly crystallized carbon were observed (scale bars: 10 nm).

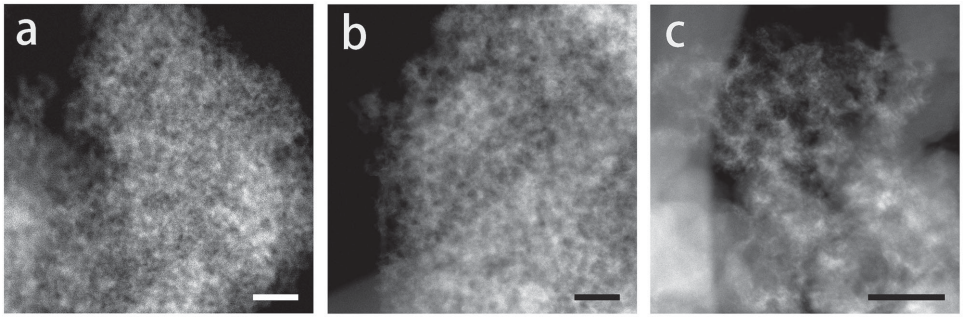

Figure 2. STEM images of a) pristine, b) fully magnesiated, and c) fully demagnesiated V_2O_5/RFC composites (scale bars: 50 nm).

and Raman spectroscopy. The contrast of STEM images is related to the *Z* number of atoms, and the differences between vanadium ($Z = 23$) and carbon ($Z = 6$) can be resolved clearly if there were isolated V_2O_5 particles. The STEM images acquired from the composite showed uniform contrast (**Figure 2**), which suggests that the supported V_2O_5 were highly dispersed in a similar manner to atomically dispersed catalysts.[26] In addition, the Raman spectrum did not show obvious peaks that could be assigned to crystalline V_2O_5 (**Figure 3**), which also suggests that the loaded metal oxide was highly dispersed and was unable to generate detectable responses.[27] The formation of this unique composite may be due to the interaction between the RFC (rich in surface defects, Figure 3a) and the nanoclusters and/or the precursors. The surface area and porosity characteristics of the composites were studied with N_2 sorption measurements (isotherm shown in Figure S1 in the Supporting Information). Both RFC and the composite have high surface area and pore volume, and could provide ample surface for efficient electrolyte diffusion and surface/near surface redox reactions. The RFC had a specific surface area and pore volume of 1188 m^2 g^{-1} and 6.3 cm^3 g^{-1}, respectively. After AHD of 45 wt% V_2O_5, the surface area and pore volume decreased to 593 m^2 g^{-1} and 2.8 cm^3 g^{-1}, respectively. The chemical composition and state of the vanadium oxides coated on carbon was identified with ^{51}V nuclear magnetic resonance (NMR) and X-ray photoelectron spectroscopy (XPS). The pristine V_2O_5/RFC composite showed a ^{51}V NMR resonance same as the crystalline sample (orthorhombic V_2O_5, Figure 3b), and this further confirms successful formation of V_2O_5 in the composite. The V 2p XPS (**Figure 4**) spectrum of the pristine material showed that the

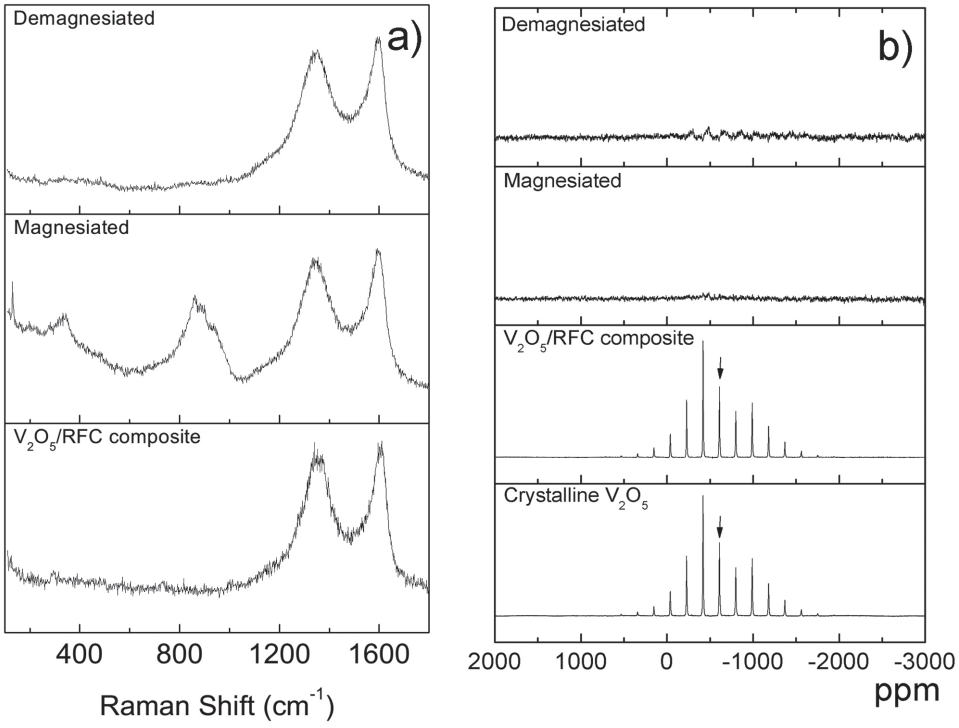

Figure 3. a) Set of Raman spectra acquired from pristine, magnesiated, and demagnesiated V_2O_5/RFC composites. The magnesiated V_2O_5 showed Raman peaks that may be assigned to magnesium vanadate whereas both pristine and demagnesiated V_2O_5 did not show obvious peaks. b) Set of MAS-NMR spectra acquired from pristine, magnesiated, and demagnesiated V_2O_5. A standard crystalline V_2O_5 was also measured for comparison. The isotropic resonances are marked with arrows.

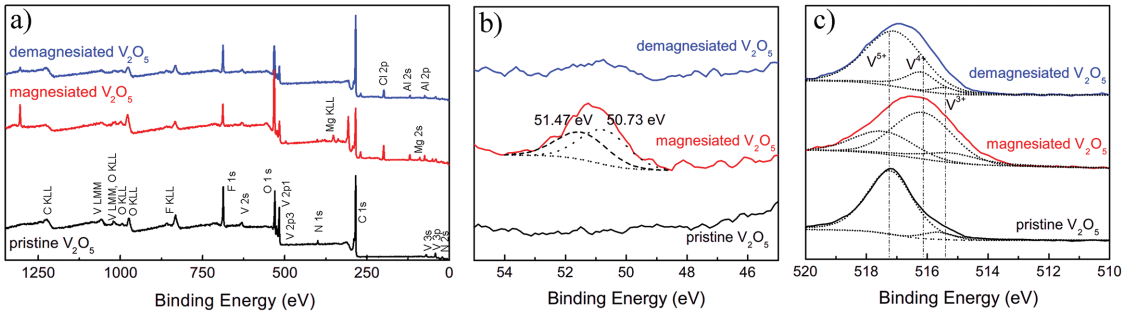

Figure 4. Set of XPS spectra acquired from pristine, magnesiated, and demagnesiated V_2O_5/RFC composites: a) Survey spectra, b) regional Mg 2p spectra, and c) V 2p spectra.

V^{5+} is the dominant species but species with lower oxidization states (V^{3+} and/or V^{4+}) were also observed with a much lower intensity.

The activity of the supported V_2O_5 nanoclusters for hosting Mg^{2+} ions was studied using the electrolyte of 0.2 M $[Mg_2(\mu\text{-}Cl)_2(DME)_4][AlCl_4]_2$ in dimethoxyethane (DME). This electrolyte has a wide voltage window that exceeds 3.0 V and has excellent activity for Mg deposition and stripping.[6b] The working electrodes were prepared by casting the slurry made with the composite (80 wt%), conductive carbon (10 wt%) and polyvinylidene fluoride (PVDF, 10 wt%) on a piece of carbon paper. We first used the galvanostatic charge–discharge technique to evaluate the material using a two-electrode setup (with Mg metal as the counter/reference electrode, see the Supporting Information for details). The composites exhibited a nearly linear voltage profile as a function of the reaction time (i.e., reacted Mg^{2+} ions) in the voltage window of ≈0.5–2.8 V. This suggests a pseudocapacitive energy storage process (discussed in detail below), and overall a high initial discharge capacity of 180 mAh g^{-1} was obtained at 40 mA g^{-1} (based on weight of the composite, ≈350 mAh g^{-1} based on V_2O_5, Figure S2, Supporting Information). Such a pseudocapacitive capacity is comparable or even higher than the battery type V_2O_5 electrode materials established for lithium ion batteries and sodium ion batteries,[22c,28] and is among the highest for all cathode materials developed for Mg batteries that are based on intercalation and/or conversion mechanism.[1a,3a,11b,29] During subsequent cycles the composite electrode had capacity fade and decreased to ≈90 mAh g^{-1} (composite, or ≈160 mAh g^{-1} V_2O_5) after ≈five cycles (Figure S2, Supporting Information), and the possible reasons will be discussed below. Besides these electrochemistry results, the reversible uptake of Mg^{2+} ions was also confirmed from the combined imaging and spectroscopy analysis with STEM, XPS, EDS, and Raman techniques (Figures 2–4). The Raman spectrum of the magnesiated electrode shows broad peaks centered at 980 and 370 cm^{-1} that could be assigned to magnesium vanadate (Figure 3).[30] The magnesiated V_2O_5, however, was still amorphous as observed from the electron diffraction and STEM observations (Figure 1 and Figure 2). After a complete demagnesiation process, the V_2O_5 returned to the original state, and the Raman and STEM/TEM results are similar as the pristine material (Figure 1 and Figure 2). Figure 3b shows a set of ^{51}V NMR characterization results. It is interesting to note that there were dramatic changes in the NMR spectra upon magnesiation and demagnesiation, and significantly decreased resonance intensity and resolution was observed. This is similar to observations of lithium intercalation with V_2O_5, and can be attributed to a first order electronic transition with charge ordering and the formation of localized vanadium ions.[31]

The reversible storage of Mg ions was also confirmed with XPS and EDS. Figure 4 shows a set of survey and regional XPS spectra acquired from pristine, magnesiated, and demagnesiated V_2O_5 samples. The survey spectra and the corresponding atomic ratios (Table S1, Supporting Information) reveal reversible changes in Mg content upon magnesiation and demagnesiation, and the atomic ratio of Mg with respect to V decreased from ≈75% for the magnesiated electrode to ≈8% for the demagnesiated electrode. Such reversible changes were also observed with the EDS spectra shown in Figure S3 in the Supporting Information. The high-resolution XPS scan of Mg 2p spectra supports this reversible behavior (Figure 4b), and interestingly the fully magnesiated electrodes showed one broad peak that can be best fitted with two component peaks. This suggests nonuniformity in the local Mg ion binding environment and probably centered with two conditions at 50.73 and 51.47 eV. The V 2p spectra (Figure 4c) reveals reversible changes in the oxidization state of vanadium. The pristine V_2O_5 material exhibited predominately the V^{5+} oxidation state. The uptake of Mg ions is accompanied with the appearance and increases of the V^{4+} peak at 516.6 eV and V^{3+} peak at 515.3 eV. Upon demagnesiation the intensity for both V^{4+} and V^{3+} peaks was decreased whereas the V^{5+} peak was increased. This clearly suggests that vanadium was participating in the magnesiation and demagnesiation reactions.[32]

The electrochemistry and battery performance data are shown in **Figure 5**. Figure 5a shows a set of CV results collected at scan rates from 2 to 50 mV s^{-1} using a three-electrode setup, with two Mg strips working as the reference and the counter electrodes, respectively. The composite electrode exhibited broad cathodic and anodic responses. Noticeably, the current densities were significantly higher than either the RFC alone or bulk V_2O_5 (Figure 5b; Figures S4 and S5, Supporting Information), suggesting significantly improved electrochemical activities with the composite material. The CVs at different scan rates were analyzed and nearly linear relationships between the current (cathodic at 1.0 V and anodic at 2.4 V) and the scan rate were determined (Figure 5a, inset). Such a relationship suggests that the electrochemical reaction was surface limited (as opposed to diffusion limited) and can be described

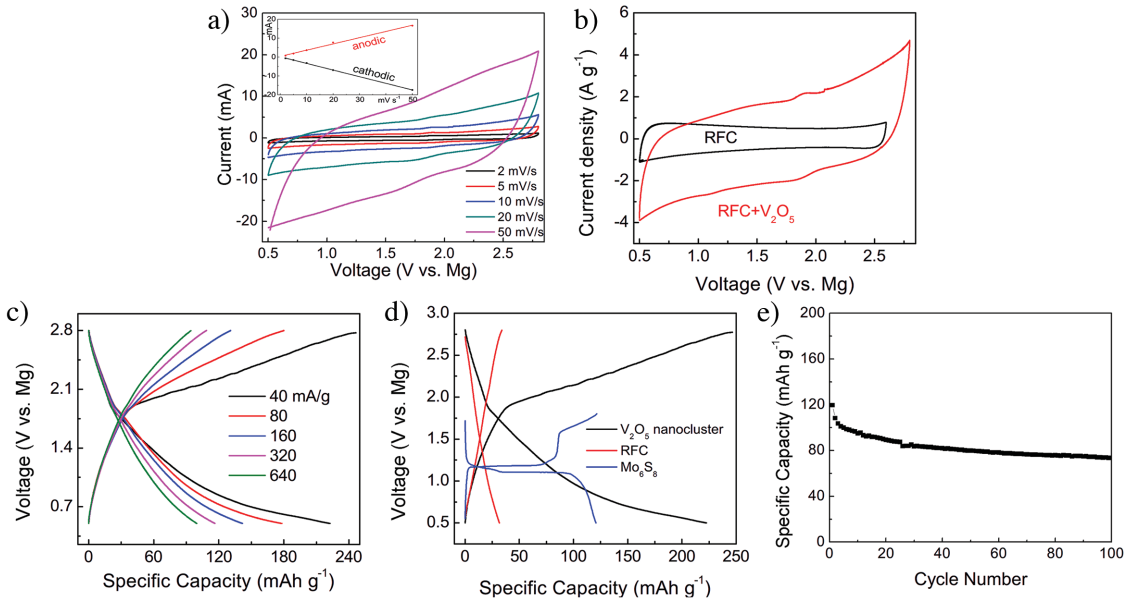

Figure 5. Electrochemical results of V_2O_5/RFC composites in 0.2 M $[Mg_2(\mu\text{-}Cl)_2(DME)_4][AlCl_4]_2$: a) Cyclic voltammetry at different scan rates, the inset shows a linear relationship between scan rates and currents that is characteristic of surface limited electrochemical reaction, b) comparison of the CV curves (at 10 mV s^{-1}) for RFC only and RFC/V_2O_5 composite, c) rate performance of the composite, d) comparison of the specific capacity of RFC, Mo_6S_8, and V_2O_5 for Mg battery cathode, and e) cyclic stability of RFC/V_2O_5 composite at 320 mA g^{-1}.

as a pseudocapacitive process, and this type of reaction usually offers excellent rate capability.[33] The rate performance of the composite was indeed excellent, and the capacity was maintained at ≈100 mAh g^{-1} even at a high current density of 640 mA g^{-1} (Figure 5c). Figure 5d compares the activity of the composite material with typical cathode materials developed for Mg batteries, including the Chevrel phase Mo_6S_8 (<2.0 V, ≈120 mAh g^{-1})[10a] and RFC (2.8 V, ≈30 mAh g^{-1}) at similar current densities. The comparison clearly suggests that the composites based on nanoclusters have the highest capacity and voltage and therefore hold great promises for the future.

In strong contrast with the supported V_2O_5 nanoclusters, both bulk crystalline V_2O_5 and RFC alone exhibited much smaller capacity when tested under identical conditions (Figure 5; Figures S4 and S5, Supporting Information). This suggests that the phase of V_2O_5 plays critical roles on hosting Mg^{2+} ions. To gain better understanding on the reaction mechanism, we studied the effect of annealing in H_2/Ar atmosphere on the electrochemical behavior of V_2O_5/RFC. The annealing process induces the aggregation of nanoclusters and formation of larger particles as evidenced by the XRD patterns and TEM images (**Figure 6**a,b). It is interesting to note that in contrast to the synthesis of V_2O_5 with the conventional sol–gel processes that annealing at 300 °C is high enough to obtain crystalline V_2O_5,[34] the presence of carbon support and carbon–V_2O_5 nanoclusters interaction strongly prohibited the crystallization and no clear lattice was developed below 600 °C (Figure 6c). Therefore, the sample annealed at 900 °C was used for electrochemical tests. The high Mg^{2+} ion storage capacity of the composites was mostly retained after annealing as evidenced from the CV results (Figure 6d). After careful examination of the high-resolution TEM images of the composite, it appears that the crystalline vanadium oxides were thin plates anchored on carbon (Figure 6b) and hence the surface Mg ion storage process should still stand, and this may explain the electrochemical activity. Additionally, we also studied an alternative electrolyte to rule out the possibility of side reactions since the $[Mg_2(\mu\text{-}Cl)_2(DME)_4][AlCl_4]_2$ electrolyte has very complicated solution chemistry. In this case, we used 0.4 M $Mg(TFSI)_2$ in diglyme that is representative for conventional and simple battery electrolytes, and the results show responses similar as in the Mg battery electrolyte (Figure S6, Supporting Information). This suggests that the observed electrochemical responses were indeed originated from reactions with Mg ions.

The exceptionally high capacity and high rate behavior of V_2O_5 nanoclusters and the combined spectroscopy and microscope characterizations suggest the presence of a unique energy storage mechanism that maybe best described as the "molecular storage mechanism". In reference to the well-documented sol–gel synthesis mechanism of oxides and the interface growth mechanism of monolayer V_2O_5 on supported substrates,[27,35] we believe the AHD method of synthesizing carbon supported V_2O_5 nanoclusters results in 1D, 2D, and 3D V_2O_5 nanoclusters that are quite complex in local structure (a simplified model to illustrate the interface is shown in **Figure 7**) but share the important characteristics of nanoclusters. The formation of such an interface may be assisted by the surface chemistry of RFC because it has rich defective and reactive sites (such as sp^3 carbon and surface functional groups, Figure 3a) in comparison with more graphitized carbon materials such as graphene and carbon nanotubes. These surface supported molecular nanoclusters have reactive sites and could react with Mg ions through reversible chemical binding reactions (Figure 7). This reaction is mostly

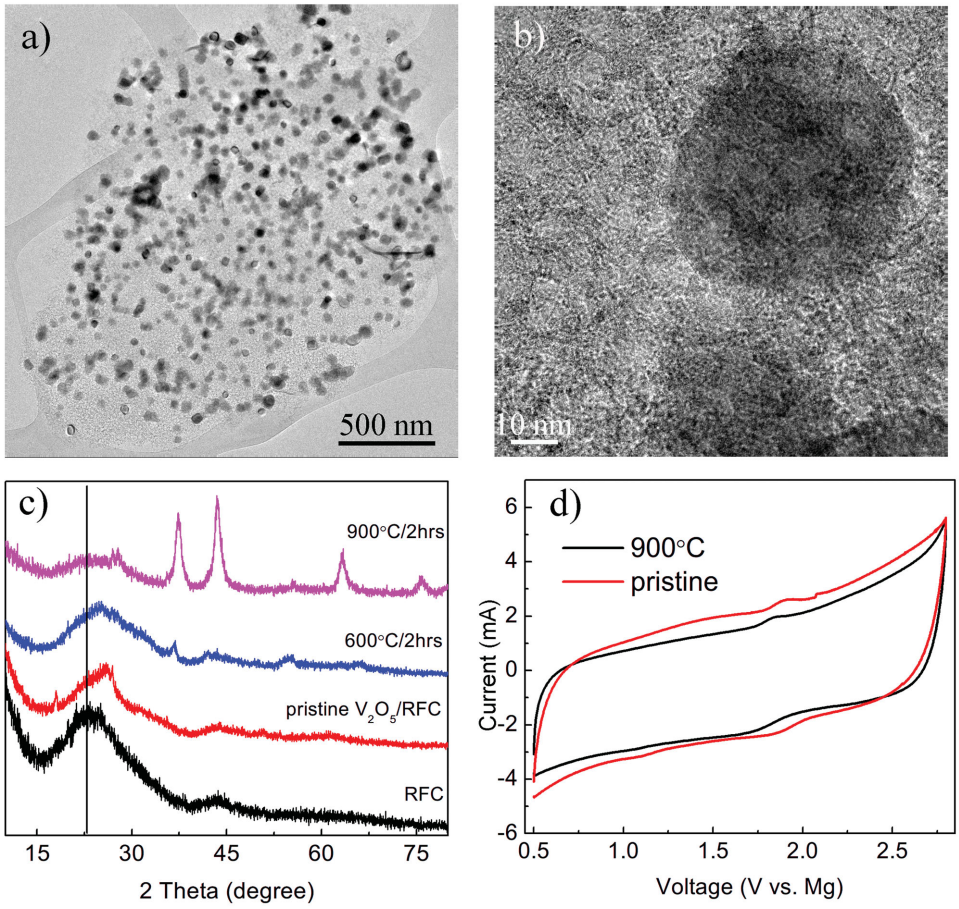

Figure 6. Effect of annealing on the behavior of V_2O_5 nanoclusters: a,b) TEM images after annealing at 900 °C, c) XRD patterns for RFC and V_2O_5/RFC composites annealed at different temperatures, and d) comparison of the CV profile of composites before and after annealing at 900 °C, the scan rate was 10 mV s^{-1}.

surface oriented and does not involve substantial solid-state Mg^{2+} ion transport and leads to the capacitive behavior with outstanding rate performance. The drawback of this molecular mechanism for this composite material, however, is the stability over repeated battery cycles and the capacities only retained ≈90 mAh g after 50 cycles (Figure 5e for stablity at 320 mA g^{-1} and Figure S2 for stability at 40 mA g^{-1}). A possible reason is that the molecular interactions of V_2O_5–carbon and magnesiated/demagnesiated V_2O_5–carbon may have very different strength, as can be seen from Raman spectra, and repeated magnesiation cycles may lead to detachment of the nanoclusters. Composites with stronger nanoclusters–carbon support interaction, such as through controlled synthesis and/or tune of carbon surface chemistry, may have improved stability.

3. Conclusion

In summary, we report a strategy for development of magnesium cathode materials using supported nanoclusters that implement a molecular energy storage mechanism. The unique structure of the V_2O_5 nanoclusters identified in this work allows a reversible reaction with Mg ions and results in the composite delivering superior reaction kinetics compared with bulk crystalline materials. The results described here suggest the critical importance of phase and dimensionality for Mg ion host materials. Even though the cyclic stability needs further improvement, by methods such as modification of carbon support chemistry and support-nanocluster interactions, the approach and results discussed in this paper provide a viable approach for high-voltage and high-capacity Mg batteries.

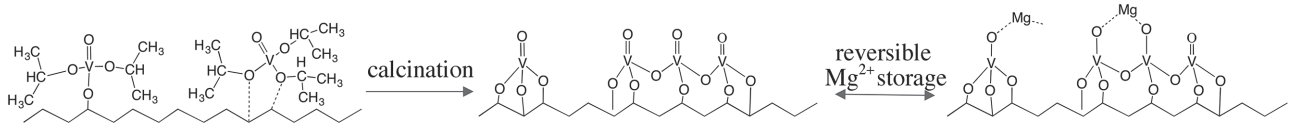

Figure 7. Proposed surface mechanism for the formation of highly dispersed vanadium oxide nanoclusters on a porous carbon support and the molecular reversible storage of Mg ions.

4. Experimental Section

Material Preparation and Characterization: In a typical procedure, RFC (50 mg) was first degassed and loaded with water by exposing to water vapor at 80 °C for one hour. The ambient hydrolysis deposition (AHD) of V_2O_5 was conducted by dispersing the water loaded RFC in a diluted solution of vanadium(V) trisisopropoxide in cyclohexane (10 vol%). The mixed dispersion was aged for one hour and was then filtered inside a glovebox. The solid products collected were heated at 225 °C in air for 2 h. The above AHD cycle was repeated to achieve the desired V_2O_5 loading.

XRD analysis was conducted using a Rigaku MiniFlex II instrument. TEM images were acquired using an FEI Tecnai G^2 (200 kV field-emission gun) transmission electron microscope. S/TEM images were acquired with a Cs-corrected FEI Titan (300 kV field emission gun). The EDS spectra were acquired with an EDAX Sapphire energy dispersive X-ray spectrometer fitted to the Cs-corrected 300 kV FEI Titan. The ^{51}V solid-state NMR spectra were obtained at a Larmor frequency of 157.65 MHz on a 600 MHz (14.1 T) NMR spectrometer (Agilent, USA) equipped with a 1.6 mm HXY triple-resonance magic angle spinning (MAS) probe and a spinning speed of 30 kHz. The sample was transferred to the NMR rotor inside a glovebox and the rotor was kept in a sealed container to minimize air exposure. All MAS–NMR experiments were performed using dry nitrogen gas. Raman spectra were obtained on an inverted microscope (Nikon Eclipse Ti) coupling with Raman spectroscopic system (Horiba Jobin Yvon). Red He–Ne laser (632.8 nm) was used as the excitation laser source.

Electrochemistry: The electrodes were prepared as follows: 80 wt% V_2O_5 /RFC composite, 10 wt% super-P carbon and 10 wt% PVDF were mixed as slurry using N-methyl-2-pyrrolidone as the dispersant. The slurry was coated on a piece of carbon paper. Typical active material loading was ≈3 mg cm^{-2}. The electrolyte solution was 0.2 M $[Mg_2(\mu\text{-}Cl)_2(DME)_4][AlCl_4]_2$ in DME, prepared by following the reported protocol of reacting aluminum chloride with magnesium chloride in DME.[6b] The batteries for cell testing were assembled inside an Ar-filled glovebox as Swagelok cells, using glass fiber paper as the separator, a piece of Mg metal as the anode, and molybendum metal as the cathode current collector. Cyclic voltammetry (CV) tests were conducted using a CHI660C electrochemical workstation (CH instrument, US). Charge–discharge and cyclic stability tests were conducted using a Land battery analyzer.

Supporting Information

Supporting Information is available from the Wiley Online Library or from the author.

Acknowledgements

This research was supported by U.S. Department of Energy, Office of Science, Basic Energy Sciences, Division of Material Sciences and Engineering, under Award KC020105-FWP12152. The (S) TEM and NMR studies were supported as part of the Joint Center for Energy Storage Research (JCESR), an Energy Innovation Hub funded by the U.S. Department of Energy, Office of Science, Basic Energy Sciences. (S) TEM, XPS, NMR, and Raman experiments were conducted at the William R. Wiley Environmental Molecular Sciences Laboratory (EMSL), a national scientific user facility sponsored by the DOE's Office of Biological and Environmental Research and located at PNNL. PNNL is operated by Battelle for the Department of Energy under Contract No. DE-AC05-76RLO1830. V.R. and X.J. acknowledge support from the Oregon State University Venture Development Fund.

Received: December 21, 2015
Revised: February 5, 2016
Published online: April 13, 2016

[1] a) D. Aurbach, Z. Lu, A. Schechter, Y. Gofer, H. Gizbar, R. Turgeman, Y. Cohen, M. Moshkovich, E. Levi, *Nature* **2000**, *407*, 724; b) H. Yoo, I. Shterenberg, Y. Gofer, G. Gershinsky, *Energy Environ. Sci.* **2013**, *6*, 2265.
[2] J. Muldoon, C. B. Bucur, T. Gregory, *Chem. Rev.* **2014**, *114*, 11683.
[3] a) T. Gao, M. Noked, A. J. Pearse, E. Gillette, X. Fan, Y. Zhu, C. Luo, L. Suo, M. A. Schroeder, K. Xu, S. B. Lee, G. W. Rubloff, C. Wang, *J. Am. Chem. Soc.* **2015**, *137*, 12388; b) N. Wu, Z.-Z. Yang, H.-R. Yao, Y.-X. Yin, L. Gu, Y.-G. Guo, *Angew. Chem.* **2015**, *127*, 5849.
[4] a) J. Muldoon, C. B. Bucur, A. G. Oliver, T. Sugimoto, M. Matsui, H. S. Kim, G. D. Allred, J. Zajicek, Y. Kotani, *Energy Environ. Sci.* **2012**, *5*, 5941; b) C. J. Barile, E. C. Barile, K. R. Zavadil, R. G. Nuzzo, A. A. Gewirth, *J. Phys. Chem. C* **2014**, *118*, 27623.
[5] O. Mizrahi, N. Amir, E. Pollak, O. Chusid, V. Marks, H. Gottlieb, L. Larush, E. Zinigrad, D. Aurbach, *J. Electrochem. Soc.* **2008**, *155*, A103.
[6] a) R. E. Doe, R. Han, J. Hwang, A. J. Gmitter, I. Shterenberg, H. D. Yoo, N. Pour, D. Aurbach, *Chem. Commun.* **2014**, *50*, 243; b) Y. Cheng, R. M. Stolley, K. S. Han, Y. Shao, B. W. Arey, N. M. Washton, K. T. Mueller, M. L. Helm, V. L. Sprenkle, J. Liu, G. Li, *Phys. Chem. Chem. Phys.* **2015**, *17*, 13307.
[7] O. Tutusaus, R. Mohtadi, T. S. Arthur, F. Mizuno, E. G. Nelson, Y. V. Sevryugina, *Angew. Chem. Int. Ed.* **2015**, *54*, 7900.
[8] Y. Cheng, T. Liu, Y. Shao, M. H. Engelhard, J. Liu, G. Li, *J. Mater. Chem. A* **2014**, *2*, 2473.
[9] a) S. Yagi, T. Ichitsubo, Y. Shirai, S. Yanai, T. Doi, K. Murase, E. Matsubara, *J. Mater. Chem. A* **2014**, *2*, 1144; b) E. Levi, Y. Gofer, D. Aurbach, *Chem. Mater.* **2010**, *22*, 860.
[10] a) Y. Cheng, L. R. Parent, Y. Shao, C. Wang, V. L. Sprenkle, G. Li, J. Liu, *Chem. Mater.* **2014**, *26*, 4904; b) R. Zhang, F. Mizuno, C. Ling, *Chem. Commun.* **2015**, *51*, 1108.
[11] a) T. S. Arthur, R. Zhang, C. Ling, P.-A. Glans, X. Fan, J. Guo, F. Mizuno, *ACS Appl. Mater. Interfaces* **2014**, *6*, 7004; b) R. Zhang, T. S. Arthur, C. Ling, F. Mizuno, *J. Power Sources* **2015**, *282*, 630.
[12] C. Ling, R. Zhang, T. S. Arthur, F. Mizuno, *Chem. Mater.* **2015**, *27*, 5799.
[13] R. E. Doe, C. M. Downie, C. Fischer, G. H. Lane, D. Morgan, J. Nevin, G. Ceder, K. A. Persson, D. Eaglesham, US Patent No. US20130260225 A1, **2013**.
[14] Y. Liang, H. D. Yoo, Y. Li, J. Shuai, H. A. Calderon, F. C. Robles Hernandez, L. C. Grabow, Y. Yao, *Nano Lett.* **2015**, *15*, 2194.
[15] Y. Shao, M. Gu, X. Li, Z. Nie, P. Zuo, G. Li, T. Liu, J. Xiao, Y. Cheng, C. Wang, J.-G. Zhang, J. Liu, *Nano Lett.* **2014**, *14*, 255.
[16] Y. Cheng, Y. Shao, L. R. Parent, M. L. Sushko, G. Li, P. V. Sushko, N. D. Browning, C. Wang, J. Liu, *Adv. Mater.* **2015**, *27*, 6598.
[17] a) Y. Wang, G. Cao, *Adv. Mater.* **2008**, *20*, 2251; b) C. K. Chan, H. Peng, R. D. Twesten, K. Jarausch, X. F. Zhang, Y. Cui, *Nano Lett.* **2007**, *7*, 490.
[18] G. G. Amatucci, F. Badway, A. Singhal, B. Beaudoin, G. Skandan, T. Bowmer, I. Plitz, N. Pereira, T. Chapman, R. Jaworski, *J. Electrochem. Soc.* **2001**, *148*, A940.
[19] P. Novák, W. Scheifele, F. Joho, O. Haas, *J. Electrochem. Soc.* **1995**, *142*, 2544.
[20] D. Imamura, M. Miyayama, M. Hibino, T. Kudo, *J. Electrochem. Soc.* **2003**, *150*, A753.
[21] a) P. Novák, J. Desilvestro, *J. Electrochem. Soc.* **1993**, *140*, 140; b) G. Gershinsky, H. D. Yoo, Y. Gofer, D. Aurbach, *Langmuir* **2013**, *29*, 10964.
[22] a) M. Sathiya, A. S. Prakash, K. Ramesha, J. M. Tarascon, A. K. Shukla, *J. Am. Chem. Soc.* **2011**, *133*, 16291; b) I. E. Rauda, V. Augustyn, L. C. Saldarriaga-Lopez, X. Chen, L. T. Schelhas, G. W. Rubloff, B. Dunn, S. H. Tolbert, *Adv. Funct. Mater.* **2014**, *24*, 6717; c) V. Raju, J. Rains, C. Gates, W. Luo, X. Wang, W. F. Stickle, G. D. Stucky, X. Ji, *Nano Lett.* **2014**, *14*, 4119.

[23] T. S. Arthur, K. Kato, J. Germain, J. Guo, P.-A. Glans, Y.-S. Liu, D. Holmes, X. Fan, F. Mizuno, *Chem. Commun.* **2015**, *51*, 15657.
[24] S. A. Al-Muhtaseb, J. A. Ritter, *Adv. Mater.* **2003**, *15*, 101.
[25] D. S. Su , R. Schlögl, *ChemSusChem* **2010**, *3*, 136.
[26] J. H. Kwak, J. Hu, D. Mei, C.-W. Yi, D. H. Kim, C. H. F. Peden, L. F. Allard, J. Szanyi, *Science* **2009**, *325*, 1670.
[27] B. M. Weckhuysen, D. E. Keller, *Catal. Today* **2003**, *78*, 25.
[28] a) Y. Liu, M. Clark, Q. Zhang, D. Yu, D. Liu, J. Liu, G. Cao, *Adv. Energy Mater.* **2011**, *1*, 194; b) A. Pan, J.-G. Zhang, Z. Nie, G. Cao, B. W. Arey, G. Li, S.-Q. Liang, J. Liu, *J. Mater. Chem.* **2010**, *20*, 9193.
[29] Y. NuLi, J. Yang, J. Wang, Y. Li, *J. Phys. Chem. C* **2009**, *113*, 12594.
[30] a) G. Busca, G. Ricchiardi, D. S. H. Sam, J.-C. Volta, *J. Chem. Soc., Faraday Trans.* **1994**, *90*, 1161; b) X. Gao, P. Ruiz, Q. Xin, X. Guo, B. Delmon, *Catal. Lett.* **1994**, *23*, 321.
[31] C. P. Grey, N. Dupré, *Chem. Rev.* **2004**, *104*, 4493.
[32] J. Mendialdua, R. Casanova, Y. Barbaux, *J. Electron Spectrosc. Relat. Phenom.* **1995**, *71*, 249.
[33] V. Augustyn, J. Come, M. A. Lowe, J. W. Kim, P.-L. Taberna, S. H. Tolbert, H. D. Abruña, P. Simon, B. Dunn, *Nat. Mater.* **2013**, *12*, 518.
[34] Y. Wang, G. Cao, *Chem. Mater.* **2006**, *18*, 2787.
[35] L. L. Hench, J. K. West, *Chem. Rev.* **1990**, *90*, 33.